Inorganic Chemistry

pubs.acs.org/IC

Article

Electroluminescence of Tetradentate Pt(II) Complexes: O^N^N^O versus C^N^N^O Coordination

Piotr Pander,* Larissa Gomes Franca, Fernando B. Dias,* and Valery N. Kozhevnikov*

Cite This: *Inorg. Chem.* 2023, 62, 5772−5779

Read Online

ACCESS | Metrics & More | Article Recommendations | Supporting Information

ABSTRACT: Alkylation of one of the phenolic hydroxyl groups in a salen-type tetradentate ligand changes the coordination mode from O^N^N^O to the cyclometallating C^N^N^O type. The ligand was used to synthesize a new cyclometalated luminescent Pt(II) complex **2**. While in solution the complex is poorly luminescent, in the solid state the emission is reinstated, which allowed one to evaluate complex **2** as a phosphorescent emitter in organic light-emitting diodes. **2** displays external quantum efficiency (EQE) = 9.1% and a maximum luminance of 9000 cd m^{-2} in a vacuum-deposited device. We carried out comparative analysis of photo- and electroluminescence of complex **2** with O^N^N^O complex **1** and demonstrated that the similar luminescent properties of the O^N^N^O and C^N^N^O complexes are rather coincidental because they display different excited-state landscapes. Surprisingly, the two complexes display a dramatically different electrochemical behavior, with O^N^N^O coordination leading to the formation of a stable electropolymer but C^N^N^O coordination fully preventing electropolymerization.

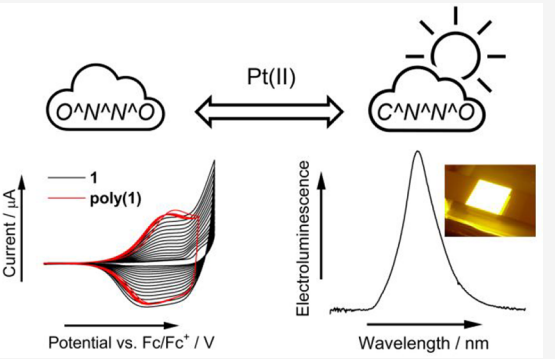

INTRODUCTION

Tetradentate platinum(II) [Pt(II)] complexes are often highly luminescent, thermally stable compounds that have been successfully used as dopants in organic light-emitting devices (OLEDs).[1] They can be used as monomolecular luminophores, where they often yield vibronically resolved luminescence, or in aggregated form as deep-red and near-infrared (NIR) emitters.[2,3] Selected Pt(II) complexes also find applications outside of OLEDs, such as in bioimaging dyes[1] or chemosensors.[4] Despite being commonly recognized for their phosphorescent properties, some may display thermally activated delayed fluorescence,[5] more known among other metal complexes, such as those of copper(I)[6] or gold(I).[7] This demonstrates that, despite years of research, Pt(II) complexes remain only partly understood, which poses a clear rationale for further studies in this subject.

Pt(II) complexes stabilized by O^N^N^O-type ligands were some of the first phosphorescent materials evaluated in OLEDs.[8] The cumulative effect of two strong σ-donor phenolate ligands deactivates the nonemissive metal-centered (MC) excited states, leading to intense luminescence. Similarly, cyclometalation is another efficient way to destabilize the MC excited states and hence to improve the luminescence. For example, tetradentate complexes of the **N^C^N^O** type with fused 6/5/5 metallocycles, in which both the phenolate and cyclometalating donor atoms are employed, are some of the best phosphorescent Pt(II) complexes known to date. The structurally similar **C^N^N^O** tetradentate Pt(II) complexes, on the other hand, are rarely investigated (the only example is complex 68 in the review by Che et al.[1]). Aggregation of square-planar Pt(II) complexes may be detrimental to their performance as OLED materials; however, certain aggregates can display intense-red and NIR luminescence.[9−12] To minimize aggregation, bulky groups such as *tert*-butyl or twisted aromatic fragments are introduced. In our recent report, we showed that two cyclopenteno rings can be introduced through intermediary 1,2,4-triazines. In this way, the planarity of the complex is compromised, leading to improved solubility as well as a better performance in the OLED in comparison with the *tert*-butyl-substituted analogue.[13] Here we show that a simple O-alkylation of one of the phenolates changes the coordination mode from O^N^N^O to C^N^N^O. This method, which is applicable to other salen-type ligands, improves the solubility of the complex in toluene, allowing solution fabrication of OLED devices. In this paper, we compare complexes **1** and **2** (Scheme 1) for applications in single-dopant OLEDs with emission color reminiscent of candlelight. The two complexes display surprisingly similar photoluminescent properties despite very different electronic structures. The differences are, however, more evident in their

Received: February 3, 2023
Published: March 30, 2023

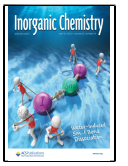

Scheme 1. Synthesis of Pt(II) Complexes 1 and 2[a]

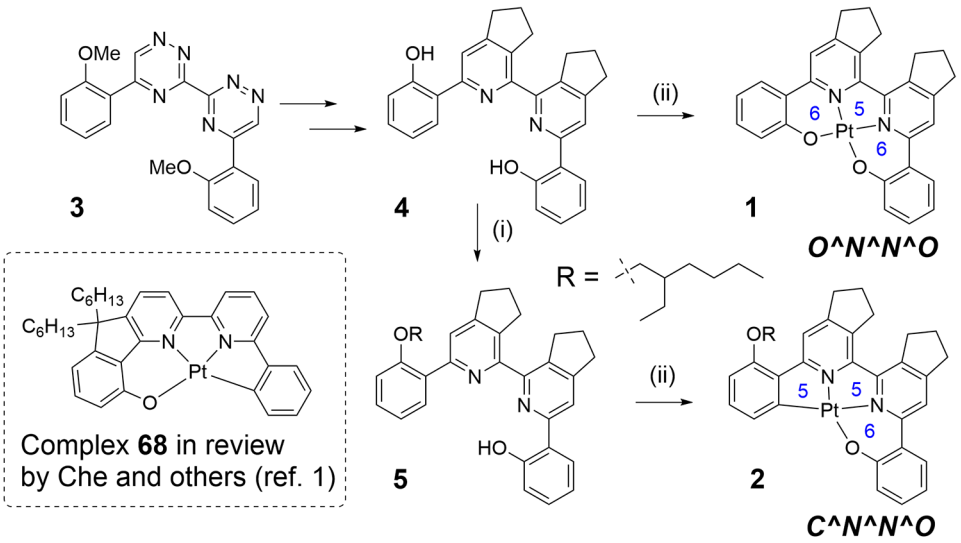

[a](i) 1-Bromo-2-ethylhexane (1 equiv), K_2CO_3, DMF, 115 °C, 14 h, 37%; (ii) $K_2[PtCl_4]$, AcOH, reflux, 14 h, 63% for **2**.

electrochemical behavior because **1** displays electropolymerization typically observed for salen-type complexes, while **2** does not.

RESULTS AND DISCUSSION

Synthesis. Synthesis of the O^N^N^O-type ligands was described earlier[13] and involved 1,2,4-triazines as intermediates (Scheme 1). The use of the 1,2,4-triazines as precursors allows an introduction of substituents by an inverse electron-demand Diels–Alder reaction. For example, two cyclopenteno units can be introduced to improve the solubility of complex **1**. To change the coordination mode from O^N^N^O to C^N^N^O, we alkylated one of the phenolic groups in **4** using 1-bromo-2-ethylhexane. The alkylation was carried out using 1 mol equiv of bromoalkene and potassium carbonate as a base in *N*,*N*-dimethylformamide (DMF) at 115 °C. We introduced the branched aliphatic chain with the aim to further improve the solubility of the complex as well as to minimize the detrimental effects of aggregation on the photophysical properties. This simple modification can be applied to other similar salen-type ligands to easily change the coordination mode from O^N^N^O with 6,5,6-metallocycles to C^N^N^O with 6,5,5-metallocycles. The alkylation, however, is not selective, and formation of the desired monoalkylated product **5** is accompanied by formation of the dialkylated product. The unreacted starting diphenol is also present in the mixture. Fortunately, the products have very different R_f values and can easily be separated by column chromatography. The isolated yield of proligand **5** was 37%. The Pt(II) complex **2** was then prepared in good yield by reaction of the proligand **5** with potassium tetrachloroplatinate in boiling acetic acid overnight.

Photophysics. To understand the differences between the C^N^N^O and O^N^N^O coordination modes, we first studied the optical properties of complex **2**. UV–vis absorption and photoluminescence (PL) spectra in solution are presented in Figure 1 and Table 1. Supplementary characteristics and PL spectra are presented in Figure S7 and Table S1. We used solvents of different polarity for the study in order to understand the excited- and ground-state properties of complex **2**. The complex displayed orange PL ($\lambda_{PL} \approx 600$ nm) and broad spectra with insignificantly resolved vibronic progression in all solvents. We observed very clear negative solvatochromism of the absorption and PL spectra onsets with increasing solvent polarity, which is similar to behavior described earlier in analogous O^N^N^O complexes.[13] This behavior is typical for complexes demonstrating pronounced metal-to-ligand charge-transfer character to the lowest excited state. The PL lifetime in solution is very short at room temperature, at around 0.2 μs, which is reflected also in a low $\Phi_{PL} \approx 0.01–0.03$, due to strong luminescence quenching. In contrast to room temperature, the PL spectrum recorded in a frozen 2-methyltetrahydrofuran (2MeTHF) glass at 77 K demonstrates a structured profile. The resultant luminescence is significantly stronger than that in liquid solutions, showing yellowish color and a longer lifetime of 11.9 μs, more typical of that presented by Pt(II) complexes.[14,15] We observed vibronic progression of around 1400 cm^{-1}, with the (0, 0) component at 561 nm being the most intense and extending out to (0, 3) at around 730 nm. The pronounced difference in the PL spectra between the liquid state and frozen glass is a manifestation of the relative flexibility of complex **2** in solution, another feature in common with the related O^N^N^O complexes.[13]

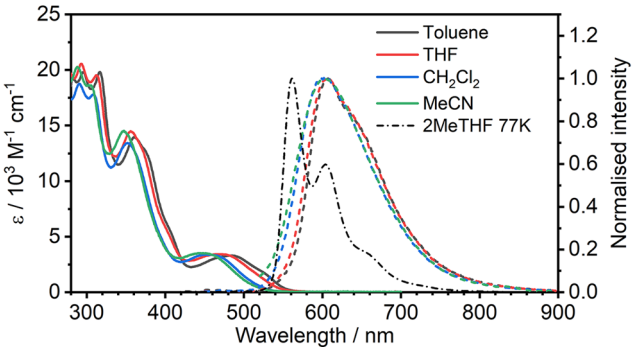

Figure 1. Absorption (solid lines) and PL (dashed lines; λ_{ex} = 365 nm) spectra of complex **2** recorded in solvents indicated in the figure legend at room temperature. The black dash-dotted line represents the PL spectrum recorded in 2MeTHF glass at 77 K.

https://doi.org/10.1021/acs.inorgchem.3c00364
Inorg. Chem. 2023, 62, 5772–5779

Table 1. Comparison of the Luminescent and Electrochemical Properties of Complexes and the OLED Performances between Analogous Complexes 1, with O^N^N^O Coordination, and 2, with C^N^N^O Coordination[a]

property		1	2
photophysics in toluene	λ_{em}/nm	624	608
	Φ_{PL}	0.24	0.02
	τ/μs	1.8	0.2
	$k_r/10^5$ s^{-1}	1.4	0.8
	$k_{nr}/10^5$ s^{-1}	0.4	49
solvent glass at 77 K	λ_{em}/nm	543, 579, 638sh	561, 605, 665sh, 730sh
photophysics in the PVK/PBD matrix	λ_{em}/nm	586	583
	Φ_{PL}	0.49	0.30
	τ/μs	5.2	4.8
	$k_r/10^5$ s^{-1}	0.9	0.6
	$k_{nr}/10^5$ s^{-1}	1.0	1.5
electrochemistry	E_{ox}/V vs Fc/Fc$^+$	0.40	0.15
	E_{red}/V vs Fc/Fc$^+$	−1.92	−1.99
	HOMO/eV	−5.50	−5.25
	LUMO/eV	−3.18	−3.11
electroluminescence in the PVK/PBD host	λ_{EL}/nm	590	582
	EQE$_{max}$/%	10.0	7.4
	L_{max}/cd m^{-2}	7000	4000

[a]Data for complex **1** were reported earlier.[13]

We studied the luminescent behavior of **2** in a popular host used for solution-processed OLEDs: a blend of poly(vinylcarbazole) (PVK) and 2-(4-biphenyl)-5-(4-*tert*-butylphenyl)-1,3,4-oxadiazole (PBD) in a 60:40 (w/w) ratio. The behavior observed in a solid film is different from that in solution. PL is blue-shifted to 583 nm (Figure S7) and much more intense (Φ_{PL} = 0.30 ± 0.10). The PL decay of **2** in a film is biexponential, with an average lifetime of 4.8 μs. This dramatic change in the PL efficiency between the liquid and solid states is due to the restriction of molecular vibrations in the solid environment. We observed a very similar radiative k_r rate in toluene (8×10^4 s^{-1}) and the PVK/PBD film (6×10^4 s^{-1}), but the nonradiative decay rate k_{nr} is ∼30-fold larger in the former: 5×10^6 s^{-1} and 1.5×10^5 s^{-1}, respectively. These results are also consistent with the behavior of complex **2** in 2MeTHF glass at 77 K. Complex **2** serves as an example that a low PL yield in solution does not disqualify the molecule as an efficient luminophore in the solid state, for example, for use as a luminescent dopant in OLEDs.

Calculations. To further the understanding of the excited-state landscape of complexes **1** and **2**, we performed density functional theory (DFT) and time-dependent DFT (TD-DFT) calculations using *ORCA*[16,17] software. Ground-state (S_0) and triplet excited-state (T_1) geometry of the complexes was optimized using B3LYP[18,19]/def2-TZVP[20]/CPCM-(toluene) for all atoms (we did not use the CPCM for the excited-state geometries), a level adequate for accurately studying metal−organic complexes. To properly model the phosphorescent properties of the complexes, we used def2-TZVP basis sets[20] corrected by zeroth-order regular approximation[21,22] for light atoms and a segmented all-electron relativistically contracted def2-TZVP basis set for Pt. We used the quasi-degenerate perturbation theory[23,24] to calculate the mixing between singlet and triplet TD-DFT states (SOC-TD-DFT). This approach was previously successfully used by us to model mono- and dinuclear Pt(II) complexes.[25] At this level of theory, we are able to model phosphorescence radiative rates[26,27] as well as the splitting of the lowest triplet (T_1) sublevels, in particular the splitting between sublevels 1 and 3, $\Delta E_{1,3}$, also known as the zero-field splitting (ZFS).[28]

Ground-State Geometry (S_0). The geometry of **1** and **2** diverges from the typical planar structure of Pt complexes involving tri- or tetradentate chelating ligands (Figure 2).[8,29]

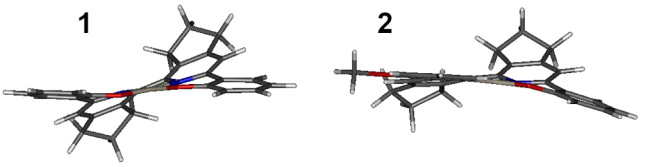

Figure 2. Optimized ground-state (S_0) geometry of complexes **1** and **2** at the B3LYP/def2-TZVP/CPCM(toluene) level.

Usually, the planar configuration around the Pt(II) center is preferred, while in the case of complexes **1** and **2**, the repulsive interaction between the two cyclopentene groups forces the complex to twist. As a result, the two "outer" phenolate units are roughly planar, but the plane is twisted with respect to the "inner" 2,2′-bipyridine fragment.

Figure 3 shows the most relevant orbitals from the standpoint of the phosphorescent properties of complexes **1**

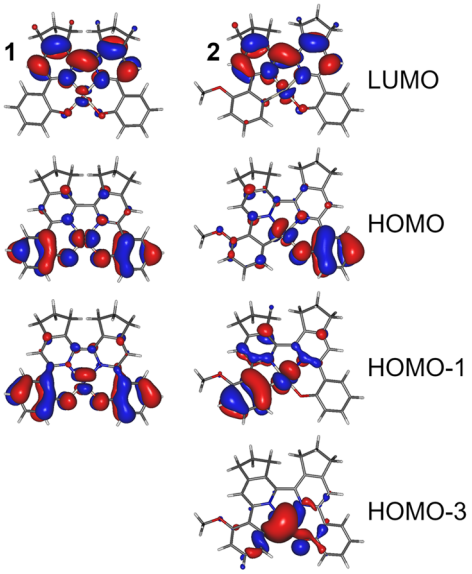

Figure 3. HOMO and LUMO isosurfaces at the S_0 geometry at the B3LYP/def2-TZVP/CPCM(toluene) level for complexes **1** and **2**.

and **2**. The highest occupied molecular orbital (HOMO) and lowest unoccupied molecular orbital (LUMO) are distributed in line with the location of the electron-rich and electron-deficient fragments of the complexes. The HOMO is localized at the O-linking phenolate units and the metal center, while the LUMO is mainly on the 2,2′-bipyridine fragment. In **1**, HOMO−1 is similar to HOMO, but with a different d orbital of the central atom, while in **2**, HOMO−1 localizes on the C-linking fragment of the ligand. For both complexes, HOMO

https://doi.org/10.1021/acs.inorgchem.3c00364
Inorg. Chem. 2023, 62, 5772−5779

and HOMO−1 involve either a d_{xz} or a d_{yz} orbital of the Pt center, while HOMO−3 in **2** is mainly localized on the d_{z^2} orbital of the metal center.

The two complexes display similar luminescent characteristics despite different types of coordination, with the predicted phosphorescence wavelengths corresponding to 666 and 649 nm, respectively for **1** and **2**. The energies of the lowest singlet states (relevant to the absorption spectrum) correspond to 620 and 597 nm, respectively.

The phosphorescent properties of the complexes originate from the mixing of singlet and triplet states by "borrowing" their radiative rates.[30] The coupling between singlet and triplet states can be described by the spin−orbit coupling matrix element (SOCME), also presented as $\langle T_n|H_{SO}|S_m\rangle$, while the most relevant couplings are with the states of relatively similar energy. The $\langle T_1|H_{SO}|S_1\rangle$ in complex **1** is relatively small, at only 7 cm^{-1}, consistent with the similar orbital geometry between the T_1 (1.780 eV) and S_1 (1.927 eV) states (both predominantly of HOMO → LUMO character). T_1, however, couples stronger with S_2 (2.377 eV), $\langle T_1|H_{SO}|S_2\rangle$ = 468 cm^{-1} because the latter is predominantly of HOMO−1 → LUMO character involving a different d orbital of the metal center. Upper S_n states are at ≈1 eV or more above the T_1, and coupling with them is less relevant. In complex **2**, T_1 (1.908 eV) couples stronger with S_1 (2.063 eV) than in **1**, $\langle T_1|H_{SO}|S_1\rangle$ = 192 cm^{-1}, because the two states differ in the contribution of HOMO → LUMO and HOMO−1 → LUMO transitions, while HOMO and HOMO−1 involve different d orbitals of Pt. T_1 also couples strongly with S_2 (HOMO−1 → LUMO, 2.514 eV), $\langle T_1|H_{SO}|S_2\rangle$ = 839 cm^{-1}, and S_3 (HOMO−3 → LUMO, 2.588 eV), $\langle T_1|H_{SO}|S_2\rangle$ = 1536 cm^{-1}, because they both involve a different d orbital of the metal center. It appears that, although **1** and **2** display similar phosphorescent behavior, it is only coincidental because the orbital and singlet−triplet coupling patterns are drastically different.

Triplet Excited-State Geometry (T_1). Estimating the phosphorescence radiative rates from the ground-state (S_0) geometry is usually sufficient in most cases because the cost of optimizing the T_1 excited-state geometry is large. However, complexes **1** and **2** as relatively small systems can be subject to such optimization with a reasonable quantity of computational resources. From the calculation at the T_1 geometry, we estimate ZFS of 8 and 16 cm^{-1} for **1** and **2**, respectively, and an identical phosphorescence radiative rate for both at 3.3 × 10^4 s^{-1}, very close to the experimental result.

The most relevant molecular orbital isosurfaces obtained from the T_1-optimized geometries are presented in Figure S9. The T_1−S_n coupling patterns are generally similar to those at the S_0 geometry, but with slight changes to the $\langle T_n|H_{SO}|S_m\rangle$ values. In **1**, we observe a relatively weak coupling between T_1 (HOMO → LUMO, 1.366 eV) and S_1 (HOMO → LUMO, 1.529 eV), $\langle T_1|H_{SO}|S_1\rangle$ = 1 cm^{-1}, but a significantly larger coupling constant between T_1 and S_2 (HOMO−1 → LUMO, 2.006 eV), $\langle T_1|H_{SO}|S_2\rangle$ = 428 cm^{-1}. Similarly, in **2**, the T_1 (HOMO → LUMO, 1.420 eV)−S_1 (HOMO → LUMO, 1.586 eV) SOCME is $\langle T_1|H_{SO}|S_1\rangle$ = 152 cm^{-1}, while the SOCME between T_1 and S_2 (HOMO−1 → LUMO, 2.219 eV) is $\langle T_1|H_{SO}|S_2\rangle$ = 741 cm^{-1}.

In conclusion, coupling between T_1 and the upper S_n states is more significant than that between S_1 and T_1. The S_1−T_1 coupling cannot on its own explain the phosphorescent properties of Pt(II) complexes because often the two lowest states share the same orbital geometry, such as in **1**.

Electrochemistry. Cyclic voltammetry (Figure 4) reveals a rather atypical redox behavior of complex **2** with both

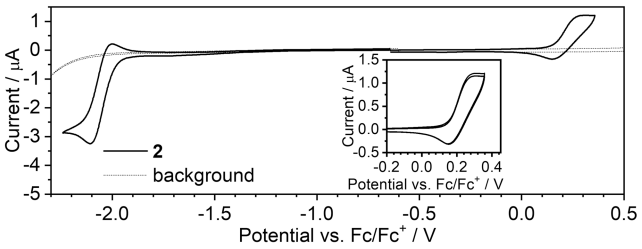

Figure 4. Cyclic voltammograms of **2** ($c = 10^{-3}$ M) recorded in 0.1 M NBu_4BF_4/CH_2Cl_2. The inset represents three cycles recorded for the first oxidation process. Scan rate = 50 mV s^{-1}.

reversible first oxidation and reduction processes. The reversibility of the reduction process is likely supported by stabilization of the resultant (radical) anions by the electron-deficient 2,2′-bipyridine unit of the ligand. The reduction onset potential of −1.99 V is similar to that reported earlier for the O^N^N^O analogues.[13] Oxidation of Pt(II) complexes is typically irreversible, mainly due to involvement of the metal center in the process; thus, reversible oxidation remains rare. Oxidation at the 0.15 V onset potential in **2** most likely involves the electron-rich part of the molecule, which is lesser communicated with the metal center. In contrast to the behavior of complex **2**, complex **1** displays irreversible oxidation.[13] We note that **2** does not display any signs of deposition of an electroactive layer on the working electrode upon oxidation. On the contrary, complex **1** appears to display deposition of a conductive layer (Figure 5a), in line with the behavior of salen-type complexes of other metals.[31,32] This behavior of complex **1** is similar to some thiophene[33,34] and carbazole[35,36] derivatives, indicating that electropolymerization is taking place in this case. We deposit a thicker layer of the polymer on the electrode by repeating multiple oxidation cycles and observe an increase in the working electrode current with each cycle (Figure 5a), which is a characteristic feature of electrodeposited conductive polymers.[37] The polymer film displays a clear and stable redox response. When subjected to reduction, it displays charge trapping (Figure 5b): negative charges become trapped within the film, only to be released upon a mildly positive potential (evident as a desorption peak at ∼0.05 V). Electropolymerization in the case of complex **1** is likely to take place through the oligomerization of cation radicals in the position para to the phenolate oxygen atom, similar to what occurs in carbazole[38] or arylamine[39] derivatives (para to nitrogen) and in agreement with the earlier accounts of metal-salen electropolymerization.[32] At the same time, **2** does not undergo a process similar to that of **1**. The C-linking arm of the ligand appears to be nonreactive, so the former would be able to form dimers at most. We believe this to be the first report of a salen-type Pt(II) complex displaying electropolymerization.

Electroluminescence. Complex **2** displays a prominent emissive behavior when used as a luminescent dopant in solution-processed and vacuum-deposited OLEDs. At first, we used a solution-processed device structure similar to that used in our earlier work[13] to facilitate a comparison with the analogous complex **1** having O^N^N^O coordination mode. The structure of this device (Dev 1) is as follows: indium−tin oxide (ITO)|Clevios HIL 1.3 (60 nm)|PVK:PBD (60:40) co

https://doi.org/10.1021/acs.inorgchem.3c00364
Inorg. Chem. 2023, 62, 5772−5779

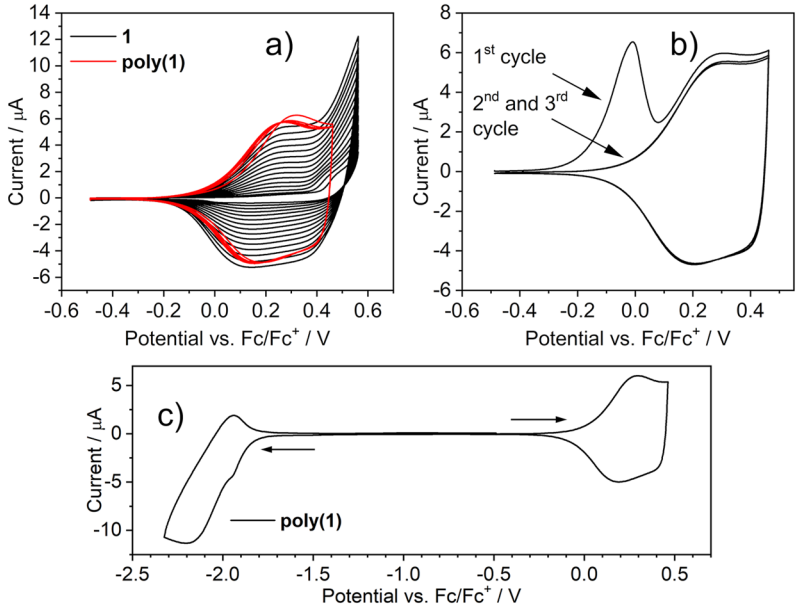

Figure 5. Cyclic voltammograms of **1** ($c = 10^{-3}$ M) and **poly(1)** recorded in 0.1 M NBu_4BF_4/CH_2Cl_2: (a) electropolymerization and electrochemical response of the electropolymer; (b) electrochemical response of the **poly(1)** film after being subjected to a reduction cycle; (c) full redox response of the **poly(1)** film. The arrows indicate the direction of potential sweep. Scan rate = 50 mV s^{-1}.

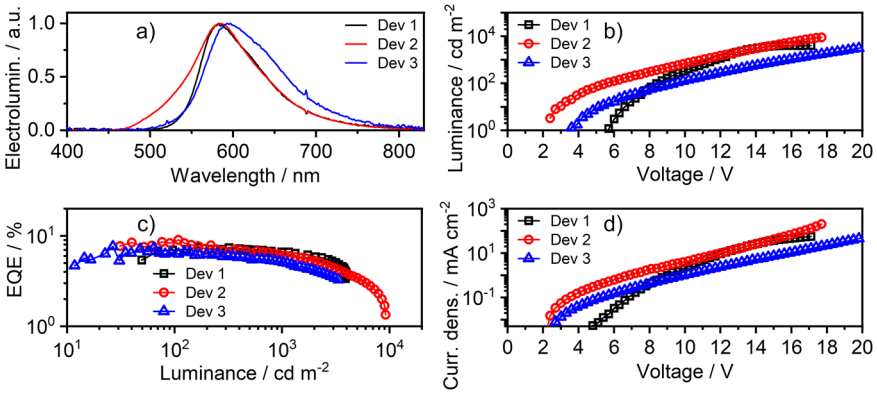

Figure 6. Characteristics of OLED devices 1−3: (a) electroluminescence spectra; (b) luminance versus applied voltage; (c) EQE versus luminance; (d) current density versus applied voltage.

5% **2** (70 nm)|TPBi (40 nm)|LiF (0.8 nm)|Al (100 nm). In this structure, Clevios HIL 1.3 acts as the hole injection and transport layer, while the PVK:PBD blend serves as the emissive layer. TPBi [1,3,5-tris(1-phenyl-1*H*-benzimidazol-2-yl)benzene] is the electron transport and LiF the electron injection layer. Electroluminescence of device 1 is representative for molecular PL of complex **2** indicating a perfect compatibility with the PVK:PBD host.

The host used in the solution-processed OLED device 1 could not be reproduced in a vacuum-deposited structure, and a careful selection led to the use of a TCTA:PO-T2T blend[40] in devices 2 and 3 (Figure 6 and Table 2). This led to the OLED architecture ITO|HAT-CN (10 nm)|TSBPA (40 nm)|TCTA (2 nm)|TCTA:PO-T2T (80:20) co *x* % **2** (20 nm)|PO-T2T (50 nm)|LiF (0.8 nm)|Al (100 nm), where $x = 5$ in device 2, while $x = 10$ in device 3. Here HAT-CN {dipyrazino[2,3-*f*:2′,3′-*h*]quinoxaline-2,3,6,7,10,11-hexacarbonitrile} serves as the hole injection layer, while TSBPA [4,4′-(diphenylsilanediyl)bis(*N*,*N*-diphenylaniline)] is the hole transport layer. We used the TCTA:PO-T2T blend as the host with an additional 2 nm exciton blocking layer of TCTA [4,4′,4-tris(carbazol-9-yl)triphenylamine]. PO-T2T {2,4,6-tris-[3-(diphenylphosphinyl)phenyl]-1,3,5-triazine} serves as the electron transport layer and LiF as the electron injection layer. Device 2 shows a small contribution of host electro-

Table 2. Characteristics of OLED Devices 1−3

	Dev 1	Dev 2	Dev 3
emitter	**2**	**2**	**2**
V_{ON}/V^a	6.6	3.0	5.3
L_{max}/cd m^{-2} ^{b}	4000	9000	3400
λ_{EL}/nm^c	582	583	593
CIE 1931 $(x, y)^d$	(0.55, 0.45)	(0.50, 0.48)	(0.58, 0.43)
CE_{max}/cd A^{-1} ^{e}	17.1	21.4	12.9
$EQE_{max}/\%^f$	7.4	9.1	7.6

^{a}Turn-on voltage at 10 cd m^{-2}. ^{b}Maximum luminance. ^{c}Electroluminescence spectrum maxima. ^{d}Color coordinates of the electroluminescence spectrum as defined in International Commission on Illumination color space CIE 1931. ^{e}Maximum current efficiency. ^{f}Maximum external quantum efficiency.

https://doi.org/10.1021/acs.inorgchem.3c00364
Inorg. Chem. 2023, 62, 5772−5779

luminescence, manifested as a shoulder at around 500−550 nm, apart from the molecular luminescence from complex **2**. Increasing the concentration of **2** in the emissive layer from 5% in device 2 to 10% in device 3 leads to elimination of the host's luminescence but leads to a red shift of the EL spectrum from 583 to 593 nm. The behavior of the EL spectrum in device 3 is likely caused by excimer or dimer formation by complex **2**, in line with some other Pt(II) complexes with a relatively planar geometry.[41]

The use of TCTA/PO-T2T allows minimization of the turn-on voltage V_{ON} from 6.6 V in the solution-processed device 1 down to 3.0 V in device 2. All three devices presented comparable characteristics, with device 2 being the most efficient, achieving an external quantum efficiency (EQE) of 9.1%. Device 2 is also the most radiant, with the maximum luminance achieving 9000 cd m^{-2}. The electroluminescence color of devices 1−3 is relatively close to that of black-body radiation with temperatures between ∼1800 and 2000 K or a candle, CIE 1931 (0.52, 0.42).[42] Complex **2** is therefore potentially useful for applications in decorative single-dopant OLED candle-imitating illumination, thanks to its relatively broadband electroluminescence.

O^N^N^O versus C^N^N^O Coordination. In this section, we aim to gather the most important similarities and differences between O^N^N^O and C^N^N^O coordination using complexes **1** and **2** as the examples (Table 1). We first note that the two complexes are relatively similar and their behavior is alike in the solid state and OLED. The most striking difference between these two complexes is in their luminescent behavior in solution. While both complexes display comparable radiative rates in toluene, around 10^5 s^{-1}, complex **2** shows a ∼100-fold larger nonradiative decay rate, resulting in a ∼100-fold lower Φ_{PL} in **2** than in the parent complex **1**. This is a manifestation of the relative rigidity between the two luminophores because the luminescence yields in solid film are very similar. Computations suggest that the similarity in the photoluminescent behavior between **1** and **2** is only coincidental because their excited-state landscapes are rather significantly different.

Another major difference between O^N^N^O and C^N^N^O coordination can be observed with cyclic voltammetry. The C^N^N^O coordination of complex **2** does not appear to have influenced the LUMO but has clearly led to destabilization of the HOMO. Complex **2** displays a 0.25 eV higher HOMO energy than its counterpart, but the difference in the LUMO energy is only 0.07 eV. The first oxidation process in **2** is reversible, which is rare in Pt(II) complexes. A reason for this behavior of **2** might be related to stabilization of the resultant (radical) cations by the phenolate fragment of the ligand. The C^N^N^O structure of complex **2** prevents electropolymerization, which is potentially an additional factor leading to the increased stability of the initial (radical) cation in **2**. This points at only the O-linking sites of the ligand to be active in the electropolymerization process, while the C-linking sites remain inactive.

Solution-processed OLEDs produced using **1** and **2** as the emissive dopants are in general very similar to each other, with their electroluminescence spectra being alike. Complex **1** appears to slightly outcompete its C^N^N^O counterpart and displays a larger maximum luminance. C^N^N^O complex **2** still requires optimization toward reducing the nonradiative effects affecting its PL quantum yield and OLED performance. However, this simple proof-of-concept study demonstrates the feasibility of this family of luminescent complexes for use in optoelectronic devices.

CONCLUSION

We have demonstrated that luminescent complexes of the C^N^N^O type can pose as prospective efficient OLED dopants, despite their modest luminescence quantum yields in solution. While the C^N^N^O proligands can easily be obtained from related O^N^N^O counterparts, this allows for additional and easy functionalization of the −OH group with alkyls or other substituents. The complex displays modest PL intensity in solution, but its luminescent performance in films is comparable with other similar complexes of the O^N^N^O type. The pseudoheteroleptic nature of complex **2** allows for better mixing between the S_n and T_1 states, which is expressed by larger SOCMEs.

We were also able to demonstrate that the structure of complex **2** prevents electropolymerization to which **1** is susceptible. Owing to the properties of complex **1**, we were able to introduce the first salen-type Pt(II) complex to undergo electropolymerization with formation of a stable electropolymer.

Complex **2** demonstrates perfect solubility, which facilitates the fabrication of solution-processed OLEDs with a maximum EQE of 7.4% and luminances of up to 4000 cd m^{-2}. Fully vacuum-deposited OLEDs yield 9.1% EQE and a maximum luminance of 9000 cd m^{-2}. This performance demonstrates the feasibility of C^N^N^O complexes for OLED applications.

In conclusion, complex **2**, being one of the very few examples of C^N^N^O coordination, poses a proof-of-concept example for the usability of these types of structures as efficient luminescent materials and luminescent OLED dopants.

ASSOCIATED CONTENT

Supporting Information

The Supporting Information is available free of charge at https://pubs.acs.org/doi/10.1021/acs.inorgchem.3c00364.

Supplementary ^1H and ^{13}C NMR spectra, experimental details, and supplementary electrochemistry, photophysics, computational, and OLED characterization results (PDF)

Cartesian coordinates (ZIP)

AUTHOR INFORMATION

Corresponding Authors

Piotr Pander − *Faculty of Chemistry, Silesian University of Technology, Gliwice 44-100, Poland; Centre for Organic and Nanohybrid Electronics, Silesian University of Technology, Gliwice 44-100, Poland;* orcid.org/0000-0003-4103-4154; Email: piotr.pander@polsl.pl

Fernando B. Dias − *Department of Physics, Durham University, Durham DH1 3LE, U.K.;* orcid.org/0000-0001-9841-863X; Email: f.m.b.dias@durham.ac.uk

Valery N. Kozhevnikov − *Department of Applied Sciences, Faculty of Health and Life Sciences, Northumbria University, Newcastle upon Tyne, Tyne and Wear NE1 8ST, U.K.;* orcid.org/0000-0001-7032-8886; Email: valery.kozhevnikov@northumbria.ac.uk

https://doi.org/10.1021/acs.inorgchem.3c00364
Inorg. Chem. 2023, 62, 5772−5779

Author

Larissa Gomes Franca − *Department of Physics, Durham University, Durham DH1 3LE, U.K.;* orcid.org/0000-0002-8089-2525

Complete contact information is available at: https://pubs.acs.org/10.1021/acs.inorgchem.3c00364

Notes

The authors declare no competing financial interest.

A version of this manuscript has been submitted to *ChemRxiv*: 10.26434/chemrxiv-2023-sjcnw.[43]

■ ACKNOWLEDGMENTS

The authors thank Yana Dikova and Prof. J. A. Gareth Williams for assistance in recording the HRMS spectrum of complex **2**.

■ REFERENCES

(1) Li, K.; Ming Tong, G. S.; Wan, Q.; Cheng, G.; Tong, W.; Ang, W.-H.; Kwong, W.-L.; Che, C. Highly Phosphorescent Platinum(II) Emitters: Photophysics, Materials and Biological Applications. *Chem. Sci.* **2016**, *7*, 1653−1673.

(2) Graham, K. R.; Yang, Y.; Sommer, J. R.; Shelton, A. H.; Schanze, K. S.; Xue, J.; Reynolds, J. R. Extended Conjugation Platinum(II) Porphyrins for Use in near-Infrared Emitting Organic Light Emitting Diodes. *Chem. Mater.* **2011**, *23*, 5305−5312.

(3) Cheng, G.; Wan, Q.; Ang, W. H.; Kwong, C. L.; To, W. P.; Chow, P. K.; Kwok, C. C.; Che, C. M. High-Performance Deep-Red/Near-Infrared OLEDs with Tetradentate [Pt(Ô N̂ Ĉ N)] Emitters. *Adv. Opt. Mater.* **2019**, *7*, 1801452.

(4) WONG, K.; YAM, V. Luminescence Platinum(II) Terpyridyl Complexes—From Fundamental Studies to Sensory Functions. *Coord. Chem. Rev.* **2007**, *251*, 2477−2488.

(5) Pander, P.; Daniels, R.; Zaytsev, A. V.; Horn, A.; Sil, A.; Penfold, T. J.; Williams, J. A. G.; Kozhevnikov, V. N.; Dias, F. B. Exceptionally Fast Radiative Decay of a Dinuclear Platinum Complex through Thermally Activated Delayed Fluorescence. *Chem. Sci.* **2021**, *12*, 6172−6180.

(6) Romanov, A. S.; Yang, L.; Jones, S. T. E.; Di, D.; Morley, O. J.; Drummond, B. H.; Reponen, A. P. M.; Linnolahti, M.; Credgington, D.; Bochmann, M. Dendritic Carbene Metal Carbazole Complexes as Photoemitters for Fully Solution-Processed OLEDs. *Chem. Mater.* **2019**, *31*, 3613−3623.

(7) Romanov, A. S.; Becker, C. R.; James, C. E.; Di, D.; Credgington, D.; Linnolahti, M.; Bochmann, M. Copper and Gold Cyclic (Alkyl)(Amino)Carbene Complexes with Sub-Microsecond Photoemissions: Structure and Substituent Effects on Redox and Luminescent Properties. *Chem. - A Eur. J.* **2017**, *23*, 4625−4637.

(8) Lin, Y.; Chan, S.-C.; Chan, M. C. W.; Hou, Y.; Zhu, N.; Che, C.-M.; Liu, Y.; Wang, Y. Structural, Photophysical, and Electrophosphorescent Properties of Platinum(II) Complexes Supported by Tetradentate N2O2 Chelates. *Chem. - A Eur. J.* **2003**, *9*, 1263−1272.

(9) Wei, Y.-C.; Wang, S. F.; Hu, Y.; Liao, L.-S.; Chen, D.-G.; Chang, K.-H.; Wang, C.-W.; Liu, S.-H.; Chan, W.-H.; Liao, J.-L.; Hung, W.-Y.; Wang, T.-H.; Chen, P.-T.; Hsu, H.-F.; Chi, Y.; Chou, P.-T. Overcoming the Energy Gap Law in Near-Infrared OLEDs by Exciton-Vibration Decoupling. *Nat. Photonics* **2020**, *14*, 570−577.

(10) Tuong Ly, K.; Chen-Cheng, R.-W.; Lin, H.; Shiau, Y.; Liu, S.; Chou, P.; Tsao, C.; Huang, Y.; Chi, Y. Near-Infrared Organic Light-Emitting Diodes with Very High External Quantum Efficiency and Radiance. *Nat. Photonics* **2017**, *11*, 63−68.

(11) Pander, P.; Sil, A.; Salthouse, R. J.; Harris, C. W.; Walden, M. T.; Yufit, D. S.; Williams, J. A. G.; Dias, F. B. Excimer or Aggregate? Near Infrared Electro- and Photoluminescence from Multimolecular Excited States of N̂ĈN-Coordinated Platinum(II) Complexes. *J. Mater. Chem. C* **2022**, *10*, 15084−15095.

(12) Rossi, E.; Colombo, A.; Dragonetti, C.; Roberto, D.; Demartin, F.; Cocchi, M.; Brulatti, P.; Fattori, V.; Williams, J. A. G. From Red to near Infra-Red OLEDs: The Remarkable Effect of Changing from X = -Cl to -NCS in a Cyclometallated [Pt(N∧C∧N)X] Complex (N∧C∧N = 5-Mesityl-1,3-Di-(2-Pyridyl)Benzene). *Chem. Commun.* **2012**, *48*, 3182−3184.

(13) Pander, P.; Bulmer, R.; Martinscroft, R.; Thompson, S.; Lewis, F. W.; Penfold, T. J.; Dias, F. B.; Kozhevnikov, V. N. 1,2,4-Triazines in the Synthesis of Bipyridine Bisphenolate ONNO Ligands and Their Highly Luminescent Tetradentate Pt(II) Complexes for Solution-Processable OLEDs. *Inorg. Chem.* **2018**, *57*, 3825−3832.

(14) Chow, P. K.; Ma, C.; To, W. P.; Tong, G. S. M.; Lai, S. L.; Kui, S. C. F.; Kwok, W. M.; Che, C. M. Strongly Phosphorescent Palladium(II) Complexes of Tetradentate Ligands with Mixed Oxygen, Carbon, and Nitrogen Donor Atoms: Photophysics, Photochemistry, and Applications. *Angew. Chemie - Int. Ed.* **2013**, *52*, 11775−11779.

(15) Gildea, L. F.; Williams, J. A. G. Iridium and Platinum Complexes for OLEDs. *Organic Light-Emitting Diodes (OLEDs)*; Elsevier, 2013; pp 77−113.

(16) Neese, F. Software Update: The ORCA Program System, Version 4.0. *WIREs Comput. Mol. Sci.* **2018**, *8* (e1327), 1.

(17) Neese, F. The ORCA Program System. *WIREs Comput. Mol. Sci.* **2012**, *2*, 73−78.

(18) Becke, A. D. Density-functional Thermochemistry. III. The Role of Exact Exchange. *J. Chem. Phys.* **1993**, *98*, 5648−5652.

(19) Stephens, P. J.; Devlin, F. J.; Chabalowski, C. F.; Frisch, M. J. Ab Initio Calculation of Vibrational Absorption and Circular Dichroism Spectra Using Density Functional Force Fields. *J. Phys. Chem.* **1994**, *98*, 11623−11627.

(20) Weigend, F.; Ahlrichs, R. Balanced Basis Sets of Split Valence, Triple Zeta Valence and Quadruple Zeta Valence Quality for H to Rn: Design and Assessment of Accuracy. *Phys. Chem. Chem. Phys.* **2005**, *7*, 3297.

(21) van Lenthe, E.; Baerends, E. J.; Snijders, J. G. Relativistic Regular Two-component Hamiltonians. *J. Chem. Phys.* **1993**, *99*, 4597−4610.

(22) van Lenthe, E.; Baerends, E. J.; Snijders, J. G. Relativistic Total Energy Using Regular Approximations. *J. Chem. Phys.* **1994**, *101*, 9783−9792.

(23) Roemelt, M.; Maganas, D.; DeBeer, S.; Neese, F. A Combined DFT and Restricted Open-Shell Configuration Interaction Method Including Spin-Orbit Coupling: Application to Transition Metal L-Edge X-Ray Absorption Spectroscopy. *J. Chem. Phys.* **2013**, *138*, 204101.

(24) de Souza, B.; Farias, G.; Neese, F.; Izsák, R. Predicting Phosphorescence Rates of Light Organic Molecules Using Time-Dependent Density Functional Theory and the Path Integral Approach to Dynamics. *J. Chem. Theory Comput.* **2019**, *15*, 1896−1904.

(25) Pander, P.; Zaytsev, A. V.; Sil, A.; Williams, J. A. G.; Lanoe, P.-H.; Kozhevnikov, V. N.; Dias, F. B. The Role of Dinuclearity in Promoting Thermally Activated Delayed Fluorescence (TADF) in Cyclometallated, N̂CN-Coordinated Platinum(II) Complexes. *J. Mater. Chem. C* **2021**, *9*, 10276−10287.

(26) Mori, K.; Goumans, T. P. M.; van Lenthe, E.; Wang, F. Predicting Phosphorescent Lifetimes and Zero-Field Splitting of Organometallic Complexes with Time-Dependent Density Functional Theory Including Spin-Orbit Coupling. *Phys. Chem. Chem. Phys.* **2014**, *16*, 14523−14530.

(27) Nozaki, K. Theoretical Studies on Photophysical Properties and Mechanism of Phosphorescence in [Fac -Ir(2-Phenylpyridine) 3]. *J. Chinese Chem. Soc.* **2006**, *53*, 101−112.

(28) Yersin, H.; Rausch, A. F.; Czerwieniec, R.; Hofbeck, T.; Fischer, T. The Triplet State of Organo-Transition Metal Compounds. Triplet Harvesting and Singlet Harvesting for Efficient OLEDs. *Coordination Chemistry Review*; Elsevier BV, 2011; pp 2622−2652.

(29) Williams, J. A. G.; Beeby, A.; Davies, E. S.; Weinstein, J. A.; Wilson, C. An Alternative Route to Highly Luminescent Platinum(II)

Complexes: Cyclometalation with N/\C/\N-Coordinating Dipyridylbenzene Ligands. *Inorg. Chem.* **2003**, *42*, 8609−8611.
(30) Baryshnikov, G.; Minaev, B.; Ågren, H. Theory and Calculation of the Phosphorescence Phenomenon. *Chem. Rev.* **2017**, *117*, 6500−6537.
(31) Tomczyk, D.; Bukowski, W.; Bester, K.; Urbaniak, P.; Seliger, P.; Andrijewski, G.; Skrzypek, S. The Mechanism of Electropolymerization of Nickel(II) Salen Type Complexes. *New J. Chem.* **2017**, *41*, 2112−2123.
(32) Łępicka, K.; Pieta, P.; Francius, G.; Walcarius, A.; Kutner, W. Structure-Reactivity Requirements with Respect to Nickel-Salen Based Polymers for Enhanced Electrochemical Stability. *Electrochim. Acta* **2019**, *315*, 75−83.
(33) Cabaj, J.; Idzik, K.; Sołoducho, J.; Chyla, A. Development in Synthesis and Electrochemical Properties of Thienyl Derivatives of Carbazole. *Tetrahedron* **2006**, *62*, 758−764.
(34) Zassowski, P.; Golba, S.; Skorka, L.; Szafraniec-Gorol, G.; Matussek, M.; Zych, D.; Danikiewicz, W.; Krompiec, S.; Lapkowski, M.; Slodek, A.; Domagala, W. Spectroelectrochemistry of Alternating Ambipolar Copolymers of 4,4′- and 2,2′-Bipyridine Isomers and Quaterthiophene. *Electrochim. Acta* **2017**, *231*, 437.
(35) Data, P.; Zassowski, P.; Lapkowski, M.; Grazulevicius, J. V.; Kukhta, N. A.; Reghu, R. R. Electrochromic Behaviour of Triazine Based Ambipolar Compounds. *Electrochim. Acta* **2016**, *192*, 283−295.
(36) Brzeczek, A.; Ledwon, P.; Data, P.; Zassowski, P.; Golba, S.; Walczak, K.; Lapkowski, M. Synthesis and Properties of 1,3,5-Tricarbazolylbenzenes with Star-Shaped Architecture. *Dye. Pigment.* **2015**, *113*, 640−648.
(37) Data, P.; Pander, P.; Lapkowski, M.; Swist, A.; Soloducho, J.; Reghu, R. R.; Grazulevicius, J. V. Unusual Properties of Electropolymerized 2,7-and 3,6-Carbazole Derivatives. *Electrochim. Acta* **2014**, *128*, 430−438.
(38) Hsiao, S.-H.; Wu, L.-C. Fluorescent and Electrochromic Polymers from 2,8-Di(Carbazol-9-Yl)Dibenzothiophene and Its S,S -Dioxide Derivative. *Dye. Pigment.* **2016**, *134*, 51−63.
(39) Data, P.; Pander, P.; Zassowski, P.; Mimaite, V.; Karon, K.; Lapkowski, M.; Grazulevicius, J. V.; Slepski, P.; Darowicki, K. Electrochemically Induced Synthesis of Triphenylamine-Based Polyhydrazones. *Electrochim. Acta* **2017**, *230*, 10−21.
(40) Shafikov, M. Z.; Pander, P.; Zaytsev, A. V.; Daniels, R.; Martinscroft, R.; Dias, F. B.; Williams, J. A. G.; Kozhevnikov, V. N. Extended Ligand Conjugation and Dinuclearity as a Route to Efficient Platinum-Based near-Infrared (NIR) Triplet Emitters and Solution-Processed NIR-OLEDs. *J. Mater. Chem. C* **2021**, *9*, 127−135.
(41) Cho, Y. J.; Kim, S. Y.; Son, H. J.; Cho, D. W.; Kang, S. O. Steric Effect on Excimer Formation in Planar Pt(II) Complexes. *Phys. Chem. Chem. Phys.* **2017**, *19*, 5486−5494.
(42) Jou, J.-H.; Su, Y.-T.; Liu, S.-H.; He, Z.-K.; Sahoo, S.; Yu, H.-H.; Chen, S.-Z.; Wang, C.-W.; Lee, J.-R. Wet-Process Feasible Candlelight OLED. *J. Mater. Chem. C* **2016**, *4*, 6070−6077.
(43) Pander, P.; Gomes Franca, L.; Dias, F. B.; Kozhevnikov, V. N. Electroluminescence of Tetradentate Pt(II) Complexes : Ô N̂ N̂ O versus Ĉ N̂ N̂ O Coordination. *ChemRxiv*, **2023**, DOI: 10.26434/chemrxiv-2023-sjcnw (accessed 2023−03−07).

https://doi.org/10.1021/acs.inorgchem.3c00364
Inorg. Chem. 2023, 62, 5772−5779